APPLICATION OF A HIGH-RESOLUTION, GROUND-BASED LASER SCANNER FOR DEFORMATION MEASUREMENTS

Stuart Gordon, Derek Lichti and Mike Stewart

Department of Spatial Sciences, Curtin University of Technology
GPO Box U1987, Perth WA 6845, Australia
Phone: +61 8 9266 2704, Fax: +61 8 9266 2703
Email: gordonsj@ses.curtin.edu.au

Abstract

Ground-based laser scanners offer a highly effective method for collecting massive volumes of precise, high-resolution 3D information for deformation monitoring applications. Unlike traditional surveying techniques that collect hundreds of discrete data points over a period of several days, laser imaging is capable of capturing several million 3D points in just a few minutes (Lichti *et al*., 2000). Multiple station imaging furnishes complete coverage of objects, deforming surfaces (such as pit walls and hazardous slopes), bridges and other structures.

This paper introduces laser scanning as an instrument which may be applicable to the field of deformation monitoring. Firstly, results of a calibration experiment are presented, providing an insight into the spatial performance of a laser scanning instrument. Secondly, results of a deformation monitoring experiment are presented. In this instance, a deforming building is simulated within a controlled environment. Finally, a report of a fieldwork exercise is given whereby a laser scanner was used to image an aging wooden bridge. This forms the basis of a preliminary investigation into the viability of using a laser scanning instrument for deformation measurements of industrial structures.

1. Introduction

Ground-based laser imaging is a rapid method of collecting millions of precisely sampled 3D points of objects over a range of 5m – 350m. This technology is relatively new and is generating interest from various industries involved in spatial data collection. Such is the predicted influence of ground-based laser scanners in the surveying industry, a major surveying firm has recently entered into this field by acquiring a leading laser scanning company. This marks the first major recognition of laser scanning technology in the traditional field of surveying and mapping.

The ability of a laser scanning instrument to collect high-resolution data over an object or surface is an advantage over traditional surveying techniques (such as total station or GPS), especially for monitoring deforming surfaces. Global coverage is acquired rather than a sparse network of discrete points. The points clouds may be quickly modelled into regular gridded or triangulated surfaces permitting local subsidence trends to be identified, which otherwise may have been missed by the traditional techniques. Additionally, signalised targets for control points are not essential in a laser scanning project. Natural features may be identified and used to register multiple scan clouds. This precludes contact with potentially unsafe terrain. This technology is applicable to surfaces, such as mine pit walls or industrial sites, such as bridges and buildings.

The greatest potential of laser scanning lies in the ability to model surfaces from the enormous archive of dense 3D point data. Industrial scenes contain features that may be modelled with geometric primitives (planes, cylinders etc.). Modelled objects can be imported into CAD or engineering software for design and analysis studies. Beraldin *et al*. (1997) reports that algorithms that rigorously fit shapes to raw points deliver a more precise determination of that object than the raw points alone.

This paper describes various experiments and field trials conducted using a commercially available 3D laser scanning system. An overview of laser scanning and data processing is presented in section 2. Section 3 reports on a calibration test performed using a camera calibration field. There are no formally recognised calibration experiments that are standard for terrestrial laser scanners of this type, since the instrumentation is relatively new. The authors are currently involved in designing and testing various experiments for this purpose. This calibration experiment is an example of one of the tests being conducted. A summary of the results from this experiment is presented herein.

A series of deformation monitoring experiments have been performed and the results presented. Section 4 documents the capture of a subsiding building face. This was a simulation activity and was undertaken on-site at Curtin University. The deformation was achieved by subjecting the laser scanner to a vertical displacement using a precision, vertical translation stage. The resulting scanner imagery was analysed for any indication of motion. Deformation vectors were determined to quantify this motion.

Section 5 describes a fieldwork exercise whereby scanning of an aging bridge was performed using multiple imaging stations. The individual scan clouds were fully mosaiced and georeferenced yielding a large 3D database of critical components within this large structure. The components were modelled and dimensions extracted for finite element analysis. This investigation highlights the superior visualisation offered with laser scanner data and also provides an insight into laser scanner project planning.

This paper concludes by remarking on the results of a spectral analysis undertaken concurrently with the fieldwork. During the processing stages of the calibration experiments and fieldwork, it was evident that various materials did not reflect the laser beam suitably as to permit a detectable return signal. This anomaly lead to holes in the datasets. In an attempt to further understand the spectral reflectance characteristics of regularly imaged materials a library of spectral signatures was generated. This information will assist future project planning stages.

2. Overview of Laser Scanning

The laser scanning system examined in this research consists of a laser source and two rotating mirrors. The distance to an object is determined by finding the two way travel time of the pulsed laser beam from the instrument to the reflecting surface. Positional information is calculated by measuring the deflection of the rotating mirrors. For a further description of imaging with coherent radiation, see Marshall (1985) and applied (aerial) laser scanning, see Baltsavias (1999).

The strength of the return signal is recorded as an intensity attribute value of each 3D point. This is a measure of the reflectance and therefore supplies information about the spectral characteristics of the object. A single session with a laser scanner may generate millions of sub-randomly distributed 3D points. The uniformity of the point distribution decreases with range, however, the precision of point determination decreases only slightly with range (Gordon *et al*., 2001). The targets shown in Figure 1 exemplify this. The target on the left was imaged nearly 8m from the instrument. The target on the right was more than 94m from the laser scanner. Both targets were populated with approximately 4000 individual 3D points. The degradation of a regular imaging pattern, possible due to atmospheric refraction, is clearly evident in Figure 1b. However, during a calibration experiment, a plane was fitted to each of these targets using least squares estimation. The deviation of points from each plane was calculated yielding an RMS of residuals for each target. The close target realised an RMS of ±3.3mm whilst the farthest target yielded an RMS of ±2.4mm (Gordon *et al*., 2001). Unfortunately, the closer target was subject to flaring caused by imaging a highly reflective object, which may have saturated the scanner's optical detector.

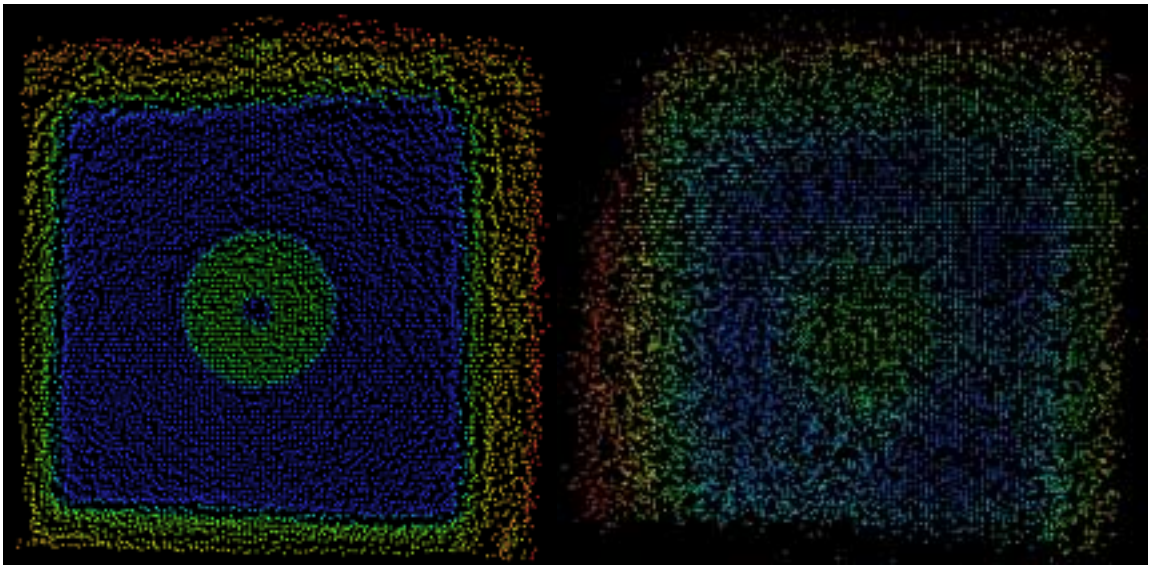

(a) (b)

Figure 1: *Laser scanner clouds of two targets 7.8m (a) and 94.8m (b) from the scanner.*

Usually one setup is not sufficient to measure an entire object. An operator must attempt numerous scans, each in a different setup position, to completely capture an object. This results in several scan clouds each referenced to a different coordinate system. To be useful, the scan clouds must be *registered* into a single coordinate system. The process of registration involves identifying common points in each overlapping scan cloud and transforming them into a single coordinate system using a six-parameter, rigid-body transformation. A local reference frame can be maintained for the duration of the monitoring campaign for comparison of successive measurement epochs.

Once registration is successfully completed, *filtering* of the cloud will remove noise from the dataset. Redundant information is also removed at this stage. For example, trees and grass on a slope may be removed to leave a clear slope. This essentially reduces file sizes and ultimately lowers processing times for modelling algorithms. The raw 3D points are then *modelled* into geometric shapes by rigorous algorithms.

All of these processes may be automated to some degree. The author is currently involved in the development of software that processes multiple clouds to deliver rigorously registered datasets that are ready for automated modelling algorithms. These modelling algorithms will fit geometric primitives by segmenting objects from the point clouds. The segmented objects may be processed by region growing algorithms. The development of automated routines will significantly reduce processing overheads of raw point clouds. All processing undertaken in this investigation has been performed on a Pentium III PC with 512mB RAM.

3. Instrument Calibration

It is important that a laser scanner undergoes a strict calibration schedule prior to operation. Calibration involves solving the internal parameters of the scanning instrument (for example, determining the optical centre) and quantifying its measuring precision and accuracy. A scanner's precision is usually expressed in terms of range precision and positional (in-plane) precision.

The laser scanner used in these studies was the Cyrax 2400 Laser Scanning System (Figure 2) built by Cyra Technologies (Oakland, USA). This instrument offers a range precision of ±4mm (1σ) and an in-plane precision of ±6mm (1σ) over an operating distance of 100m. The Cyrax scanner collects point data at a rate of 800 Hz using a green light source (central wavelength of 532nm). The maximum spatial resolution of this scanner is 0.5mm at 50m.

Figure 2 shows the Cyrax 2400 setup at a calibration site. The scanner connects to a laptop computer (shown on the larger transport case in Figure 2), which controls imaging settings, such as sampling resolution and field of view. Also shown is the power source for the laser scanner, located in the smaller transport case. The Cyrax scanning system also consists of a video-imaging device within the scanner unit. This allows the operator to capture a visual image of the terrain, from a similar viewing perspective as the laser scanner, prior to initiating the scanning session. The operator may use the video image to approximate the field of view for the scanning session using the software on the laptop computer.

Figure 2: *Cyrax 2400 Laser Scanner.*

Initial calibration testing of the Cyrax scanner was conducted on the Curtin University camera calibration wall. This wall consists of a 10m x 10m array of metallic targets that have been precisely coordinated using a total station. The scanner was setup approximately 30m from the wall. The scanning resolution was set at a nominal sampling interval of 15mm (at a range of 30m), which provided a suitably dense coverage of the wall and targets.

Once the scans were acquired, they were transformed into the calibration wall coordinate system using a six-parameter rigid body transformation. Each scan was then comparable in a single reference frame. Figure 3 is an extract from a scan cloud of the calibration wall, with the viewing perspective rotated and raised from the scanner's optical centre. The shadow effects visible in the scan cloud are caused by objects in the scanner's foreground occluding the wall. This is a fine example of the high-density information that may be generated by a laser scanning system. Moiré patterns visible on the brick wall are due to insufficient display resolution.

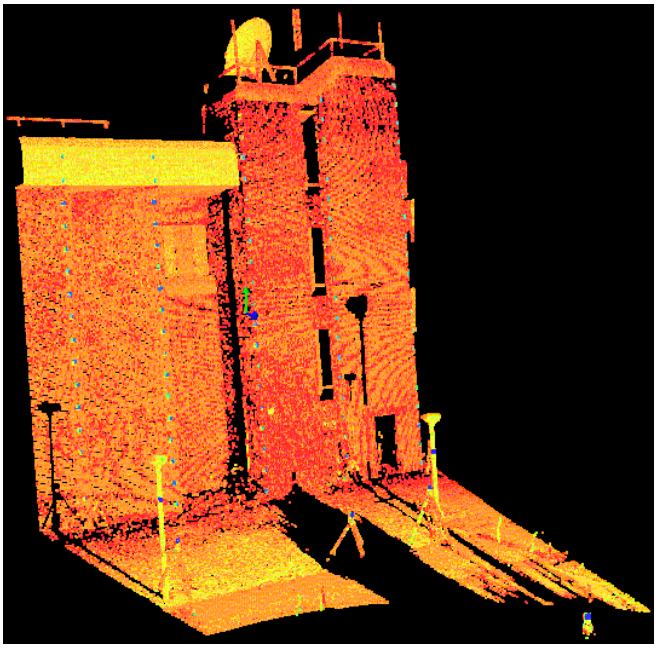

Figure 3: *Scan cloud of the camera calibration wall.*

Due to a time limitation, only five scans of the lower half of the building were captured, reducing the number of targets captured to 25. Coordinate differencing was performed between the calibrated targets and the transformed targets from the scanner data for each scan cloud. The results (Table 1) indicate that an overall RMS of residuals was found to be ±3.2mm in the X-axis and ±2.8mm in the Z-axis (in-plane axes). The range accuracy (Y-axis) was found to have an overall RMS of ±2mm. A limiting factor of this experiment is that the calibration field was poorly distributed in the range dimension. That is, the majority of the targets resided at a range of approximately 30m from the scanner.

	RMS (m)		
Sample	**X**	**Y**	**Z**
1	± 0.0034	± 0.0024	± 0.0026
2	± 0.0033	± 0.0015	± 0.0030
3	± 0.0035	± 0.0015	± 0.0028
4	± 0.0021	± 0.0017	± 0.0031
5	± 0.0035	± 0.0020	± 0.0026
Total	**± 0.0032**	**± 0.0020**	**± 0.0028**

Table 1: *RMS of coordinate differences between scanned and calibration coordinates*.

This paper briefly deals with one calibration experiment performed on the scanner. Other calibration experiments have been undertaken, since the authors are involved in developing procedures for the task of assessing the spatial (and spectral) characteristics of laser scanning systems. One such experiment used an EDM calibration baseline to assess the scanner's performance throughout its entire imaging range. For a further description regarding other calibration experiments performed and respective results, see Lichti *et al*. (2000) and Gordon *et al*. (2001).

4. Deformation Sensitivity Analysis

The next task involved assessing the sensitivity of the Cyrax laser scanner in detecting motion of a deforming object. This deformation sensitivity analysis was undertaken at Curtin University by simulating a subsiding building. The laser scanner was mounted on a precision, vertical translation stage. Five scans of the Curtin University camera calibration wall were acquired. The first two scans were 'control' epochs whereby the scanner's optical centre was held stationary. The final three scans were acquired with the scanning instrument subject to an induced vertical displacement. On each occasion, the scanner was vertically raised by 8.5mm increments. This gave the perception that the building was subsiding by that magnitude.

Once the scans were acquired, the coordinates for the centre of each target were extracted. A mean coordinate set was established for a stationary system using the first two scan clouds. This mean dataset was compared with each of the other clouds that had been subject to vertical displacement. Table 2 summarises the average movements of all 25 targets detected for each displaced epoch. The axes are in the scanner coordinate system, whereby the x-axis is horizontal in-plane and the y-axis is vertical in-plane. The z-axis, in the range direction, is positive towards the scanning instrument.

	Induced	**Mean Deformation Vectors (m)**			**Magnitude**
	ΔY (m)	**ΔX**	**ΔY**	**ΔZ**	**(m)**
Scan 3	-0.0085	-0.0062	-0.0109	-0.0017	0.0126
Scan 4	-0.0170	-0.0201	-0.0212	0.0002	0.0292
Scan 5	-0.0255	-0.0279	-0.0296	0.0036	0.0410

Table 2: *Summary of Vertical Displacements*.

Table 2 shows that a displacement, in the expected direction (Y-axis), was successfully detected. Furthermore, it was found to have the same order of magnitude as each increment of induced movement. The difference between the detected motion and the induced motion was smaller than the uncertainty of the scanner's in-plane precision. However, a horizontal movement was also detected, which occurred with the same order of magnitude as the vertical motion. Furthermore, the horizontal displacement appears to systematically grow with each epoch. This unexpected motion is believed to have been caused by dislevelment of the instrument, which has no levelling

facility. Ongoing investigations are aimed at identifying this anomaly. The movement detected in the vertical axis (ΔZ) is within the empirically determined RMS for the scanner of ±6mm.

Figure 4 presents the detected motion at each target location on the wall for the third and fourth epochs. The left graph (Figure 4a) shows the deformation vectors after the first vertical displacement increment. The graph on the right (Figure 4b) shows the vectors after the second increment. Both the induced vertical movement and horizontal systematic error are evident in the vectors. The horizontal component is more prominent in Figure 4b.

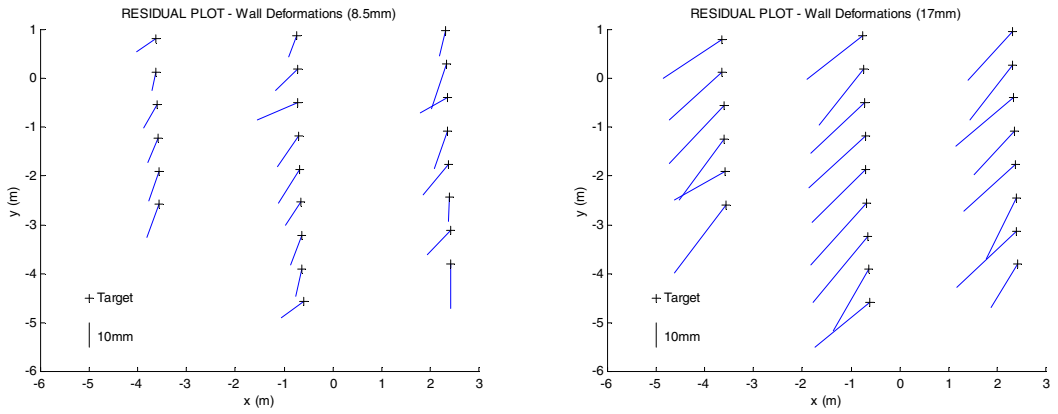

(a) (b)

Figure 4: *Deformation vectors of the subsiding building from epoch 3 (a) and epoch 4 (b).*

5. Field Trials involving Deforming Systems

Up until this stage, the application of the laser scanner has been in controlled environments whereby distances between objects and target coordinates have been precisely known. Field trials have also been conducted using real test cases. The first was an aging wooden bridge built prior to the 1950s (Figure 5). The bridge is located in Toodyay, Western Australia. It has experienced several repairs to reinforce its structure. However, it is nearing the end of its operational life and has been scheduled for destruction towards the end of 2001.

This provides an interesting test case for a number of research scientists. Curtin University structural engineers will be performing testing during critical stages of its destruction. These tests will involve loading experiments. Already, copious amounts of data have been collected using traditional engineering instruments, such as accelerometers and extensometers, for finite element analysis. It is the intention of the authors to monitor the bridge using conventional surveying techniques (total stations, photogrammetry, video *etc.*) during the structural testing. Additionally, a laser scanner will be used to collect dense information about members in the bridge.

Figure 5: *Photograph of a section of Toodyay Bridge.*

In preparation of these activities, a preliminary scanning campaign has been undertaken using the Cyrax laser scanning system. Multiple imaging stations were used to image one side of the bridge. Targets surveyed with a total station were used to provide orientation information to permit transformation of the scan clouds into a local coordinate system. Figure 6 is an example scene

extracted from the fully registered scan cloud. The final product was over 90mB of raw points describing one side of Toodyay Bridge.

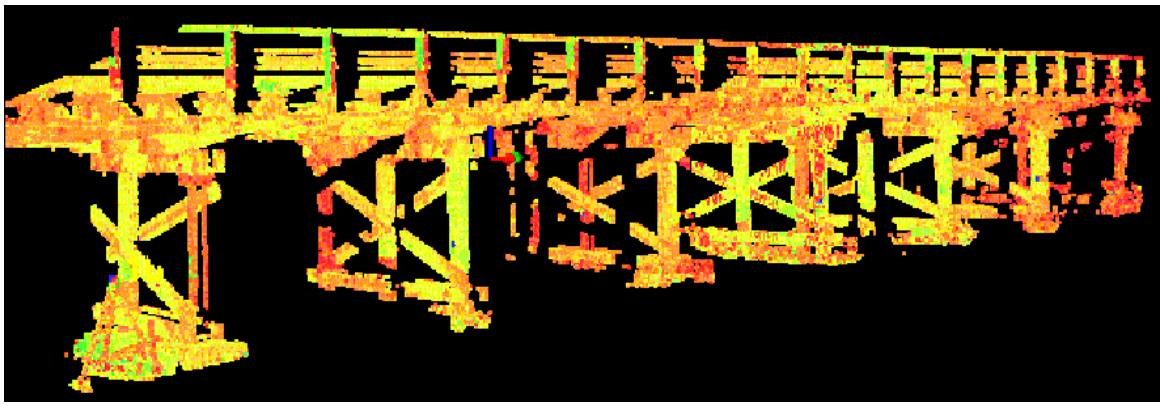

Figure 6: *Scan cloud of Toodyay Bridge*.

A manual filtering process was undertaken to remove redundant information. This included deletion of grass and light poles nearby the bridge. This process reduced the file size from 90mB to approximately 65 mB, which gives an indication of the importance of the filtering stage. This substantial saving not only increased the efficiency of the graphical display but also assisted with reducing processing overheads during the modelling process.

Various structural members were isolated from the dataset. These objects included vertical wooden columns and steel I-beams. While the steel beams could be modelled with standard modelling software provided with the scanning system, many objects could not be confidently modelled due to lack of coverage. That is, the laser scanner was set up in several locations alongside the bridge allowing imaging of only one side of the bridge. The various members that had been extracted exhibited holes. Figure 7a is an example of a vertical I-beam extracted from the dataset. Discontinuities due to occlusion are evident near the lower portion of the cloud. This problem was identified prior to commencing the project but time limitations determined the level of coverage obtainable. Examples of cross-sections taken for some of the members are shown in Figure 7b. These provided dimensional information for finite element analysis.

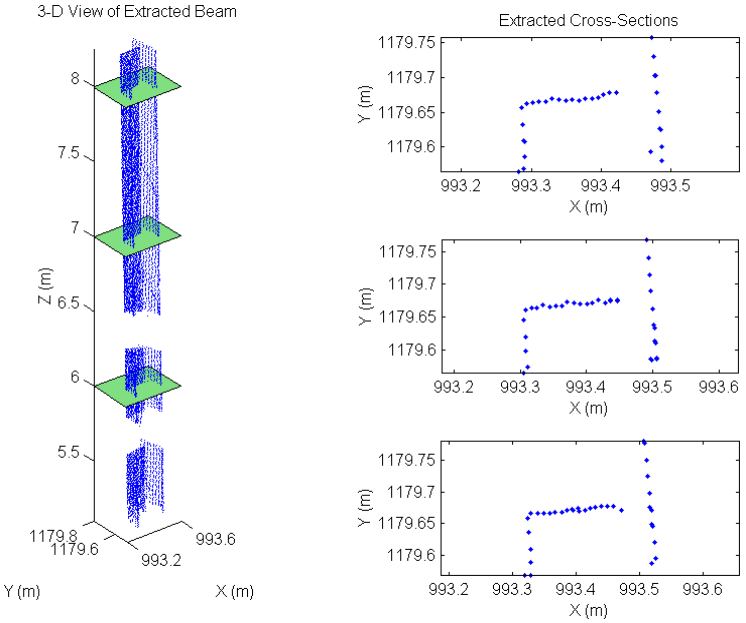

(a) (b)

Figure 7: *(a) Extracted I-beam cloud and (b) I-beam cross-sections*.

6. Spectral Reflectance Studies

During the calibration studies of the Cyrax laser scanner, the resulting scan clouds showed that some materials failed to yield a return signal. For example, holes in the dataset occurred during the scanning of the camera calibration wall, constructed of mortar and red brick clay. Figure 8 has been extracted from a scene taken during the calibration activity at this site. The mortar permitted suitable reflection of the laser beam. However, the response from the red bricks was negligible, leaving holes in the scanner cloud.

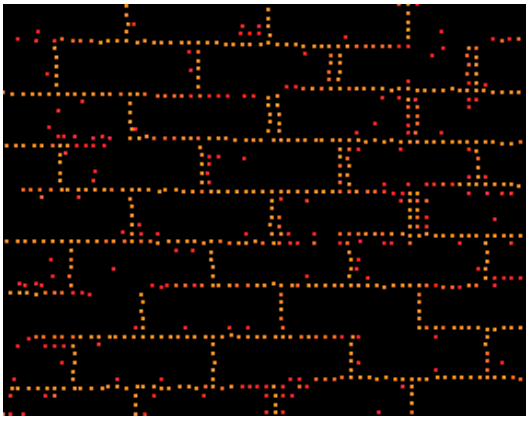

Figure 8: *Reflectance of bricks and mortar.*

During another experiment, more holes became evident as a result of various materials not suitably reflecting the green laser beam. Figure 9a is an extract from a laser scan cloud and Figure 9b is a photographic image of approximately the same scene. The numeric symbols are included for the benefit of the reader to identify similar features in each scene. Note that the concrete walkway (denoted by number 2) does not appear in the scan cloud. Furthermore, the limestone retaining wall (number 4) also fails to appear in the scanner imagery. Both objects were well within the laser scanner's operating range. Although the concrete walkway (2) is not orthogonal to the incident laser beam, the limestone retaining wall (4) is approximately normal to the beam. The only other factor that may contribute to this anomaly was that the scanner was facing direct sunlight. Therefore, the optical detector may have been saturated. However, a similar imaging scenario at Toodyay Bridge did not appear to pose such a problem. Objects 1 and 3 refer to a nearby tree and building, respectively. Both are clearly distinguishable in each scene.

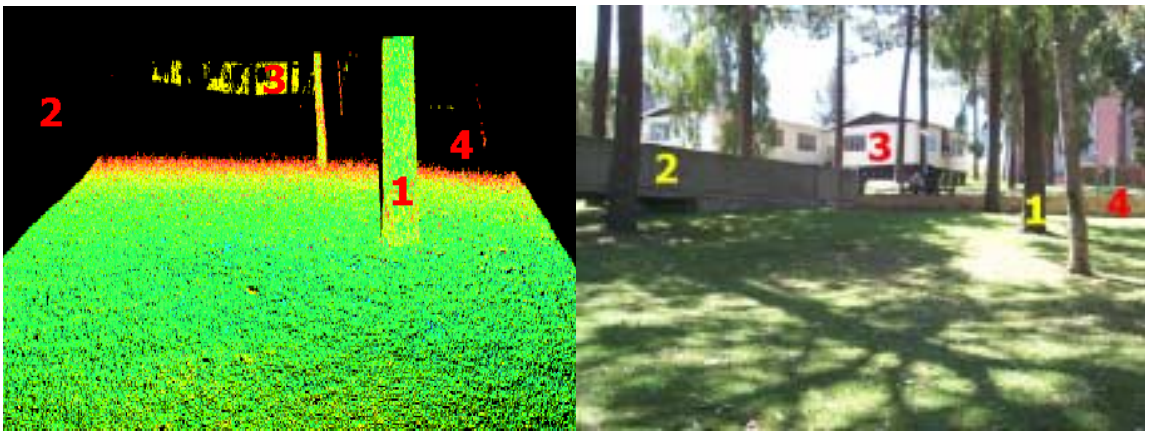

(a) (b)

Figure 9: *Scan cloud (a) and photographic image (b) of same scene.*

This deficiency of the laser to respond to all materials prompted an investigation into the spectral reflectance characteristics of common imaged material around the Curtin University campus. A library of spectral signatures was compiled using an Ocean Optics ST1000 spectrometer. This hand-held spectrometer, which was initially calibrated using a Mercury-Argon lamp, generated signatures in the spectral range of 338.4nm to 876.1nm with a sample interval of 0.525nm. Spectral reflectance signatures were measured for materials scanned with the Cyrax scanner. These included the concrete walkway and limestone retaining wall (Figure 9) and bricks and mortar (Figure 8). Sampling of the reflective targets, supplied for use with the scanner, was also

undertaken. Several samples of each object were acquired and averaged to generate a more reliable spectral signature. Figure 10 is a plot the reflectance of 4 objects over a spectral range of 400nm to 600nm. The central wavelength of the laser scanner is plotted as a dashed, vertical line.

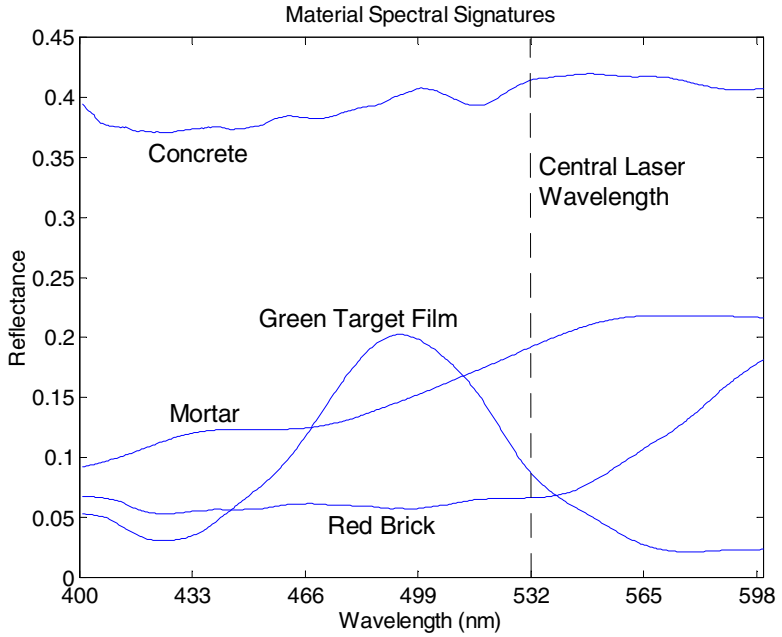

Figure 10: *Spectral Curves for Common Material.*

The lack of reflectance from the red brick can possibly be explained by the low reflectance at 532nm. As expected, the mortar offered a much higher reflectance than the bricks. However, it was unexpected that the concrete would not return the laser pulse given its relatively high and uniform spectral signature. Interestingly, the green target film supplied by Cyra was thought to peak at the same value as the central wavelength of the scanner, but the maximum was found to be slightly shifted towards the blue end of the visible spectrum.

This investigation represents a preliminary study and is not conclusive. Alternate explanations may be sought via further investigations into the performance of the scanner in full sunlight and the effect of temperature and moisture content of the scanned material. A spectral calibration of the laser scanner would also prove beneficial for maintaining spectral integrity. The spectral reflectance study was not performed at the same time as the laser scanning. Further spectral reflectance measurements are planned.

7. Conclusions

The results of preliminary field testing of a high-resolution laser scanner have been presented with respect to applications in the area of deformation monitoring. A 3D laser scanner generates large amounts of dense information describing a surface. It has been shown that this may be an advantage over traditional methods of surveying, whereby these methods generate discrete points forming a sparse network. In this scenario, local deformations may be overlooked. Furthermore, a laser scanner does not require contact with a surface, whereas traditional methods do.

The paper has demonstrated the processes involved with using a laser scanning system. Firstly, a scanning instrument must undergo a strict calibration schedule prior to use. The results from one such calibration experiment have been presented in order to give an insight into the procedures required for this exercise and to demonstrate the accuracy and precision expected from a typical laser scanning instrument. Results from this experiment reported that a range accuracy RMS of ±2.0mm (Y-axis) and in-plane accuracy of ±3.2mm (X-axis) and ±2.8mm (Z-axis) was achieved.

A workflow for a typical scanning project has been described. It commences with a project planning stage. This is influenced by the ability to maximise coverage of all objects and to minimise holes caused by occlusion of objects in the scanner's foreground. The I-beam in Figure 7 was exemplary both of these effects. The reflectance characteristics of the objects being imaged are also a concern. It has been shown that poor reflectance of certain objects leaves holes in the scan clouds. Spectral reflectance signatures may assist with project planning.

After scanning has been completed, registration is performed to mosaic all of the individual scan clouds into a large dataset with a single reference frame. Filtering removes noise and redundant information from a scene. This is beneficial for reducing file sizes and processing times. Modelling is the final stage in the processing timeline. This consists of rigorously fitting shapes to objects. Alternatively, it involves gridding or triangulating surfaces. These shapes or surfaces may then be imported into CAD or engineering software for design and analysis purposes. The author has shown that these processes may be automated to some degree. Processes such as registration may be fully automated.

Analysis of resulting scan clouds, from a simulation exercise, have shown that the Cyrax laser scanner was able to detect motion in a subsiding building wall. Furthermore, the magnitudes of the displacements detected were on the same order as those induced movements. Induced vertical motion was supplied in 8.5mm increments (*ie*. ΔY_1 = -8.5mm, ΔY_2 = -17mm, ΔY_3 = -25.5mm). The detected vertical motion was -10.9mm, -21.2mm and -29.6mm, for each epoch, respectively. A horizontal systematic error was also evident in each epoch. It was believed that this was caused by the non-vertical alignment of the instrument. The laser scanner was then applied in a field case whereby an aging bridge was imaged. The modelled objects were extracted and dimensions derived for structural analysis purposes. Future fieldwork will involve monitoring the bridge during a controlled loading and destruction experiment.

Acknowledgments

The authors gratefully acknowledge the support of Diamond River Corporation for the use of the Cyrax 2400 and Cyra Technologies for the use of an evaluation version of their visualisation software. Thanks are extended to Cindy Ong of CSIRO (Floreat, Western Australia) for the loan of the Ocean Optics hand-held spectrometer.

References

Baltsavias, E.P. (1999) "Airborne Laser Scanning: Basic Relations and Formulas", *ISPRS Journal of Photogrammetry and Remote Sensing*, Vol. 54, No. 2-3, pp. 199 - 214.

Beraldin, J-A., Cournoyer, L., Rioux, M., Blais, F., El-Hakim, S.F. and Godin, G. (1997) "Object Model Creation from Multiple Range Images: Acquisition, Calibration, Model Building and Verification", *Proceedings of International Conference on Recent Advances in 3-D Digital Imaging and Modeling*, Ottawa, Canada, May, pp. 326 - 333.

Gordon, S.J., Lichti, D.D., Stewart, M.P. and Tsakiri, M. (2001) "Metric Performance of a High-Resolution Laser Scanner", *Proceedings of SPIE Electronic Imaging 2001 Conference*, San Jose, California, February, 11 pp.

Lichti, D.D., Stewart, M.P., Tsakiri, M. and Snow, T. (2000) "Benchmark Tests on a Three-Dimensional Laser Scanning System", *Geomatics Research Australasia*, No. 72, pp. 1 - 24.

Marshall, G.F. (Ed.) (1985) *Laser Beam Scanning: Opto-Mechanical Devices, Systems, and Data Storage Optics*, Marcel Dekker, New York, USA, 425 pp.